Journal Name

ARTICLE

# Magneto-Structural Correlations in Oxalate-Bridged Sr(II)Cr(III) Coordination Polymers: Structure, Magnetization, X-band and High-Field ESR studies

Received 00th January 20xx,
Accepted 00th January 20xx

DOI: 10.1039/x0xx00000x

www.rsc.org/

L. Androš Dubraja,[a] M. Jurić,[a] J. Popović,[a] D. Pajić,[b] Y. Krupskaya,[c] V. Kataev,[c] B. Bűchner,[c] and D. Žilić*[a,c]

Results of the high-field electron spin resonance (HF-ESR) spectroscopy on the title 1D coordination polymers at frequencies up to 415 GHz, supported by X-ray, thermal, magnetic susceptibility and X-band (10 GHz) ESR studies, are presented. The heterometallic compounds $\{SrCr_2(phen)_2(C_2O_4)_4\}\cdot H_2O$ (SrCrPhen) and $\{SrCr_2(bpy)_2(C_2O_4)_4(H_2O)\}\cdot 5H_2O$ (SrCrBpy) (phen = 1,10-phenanthroline, bpy = 2,2'-bipyridine) were synthesized. Structural analysis reveals double oxalate-bridged zigzag Sr-Cr chains while magnetic susceptibility study shows paramagnetic behavior of the complexes. HF-ESR spectroscopy data were analyzed with a relevant spin-Hamiltonian yielding the *g*, *D* and *E* parameters of the Cr(III) ions. Both complexes show small magnetic easy-axis type anisotropy with $|D|$~1 K; SrCrBpy has uniaxial while SrCrPhen has biaxial anisotropy. HF-ESR study has enabled to establish rational magneto-structural correlations and revealed significant differences between very similar crystal structures. Additionally, the ability of SrCrPhen and SrCrBpy to be single-source precursors for the formation of Sr-Cr oxides was investigated.

## Introduction

Transition metal-complexes have been intensively investigated due to their wide appliances in electrical conductivity, magnetism, catalysis, gas storage and separation, electron-transfer reactions, nonlinear optics, etc.[1-4] but also for fundamental researches. In magnetism they are used, among others, for realization of low-dimensional quantum spin systems which have 0-, 1- or 2-dimensional (D) magnetic lattices formed on 3D crystal structures. For physicists, these systems are interesting because their simplicity allows comparison of theoretical models with experiments. Probably the most famous 0D quantum spin systems are compounds called single molecule magnets (SMM) because of their potentials in a field of quantum information processing.[5] SMM show magnetic hysteresis at the molecular level caused by high spin value *S* in ground state and significant magnetic anisotropy that lead to formation of barrier that keeps magnetization after removing applied magnetic field. The height of magnetic anisotropy barrier in systems with easy axis of magnetization can be expressed as $|D|S^2$ (for integer spins)[6], where *D* is axial zero-field splitting (ZFS) parameter *D* defined in spin-Hamiltonian approach.[7, 8] The barrier height could be changed by modifications of local environments such as using different ligand field, coordination ions and symmetry.[9, 10] In order to characterize complexes with desired magnetic properties, it is necessary to be able to precisely determine magnetic anisotropy.[6] Standardly used magnetic characterization techniques such as static magnetic susceptibility measurements and electron spin resonance (ESR) spectroscopy that uses commercial spectrometers (below 100 GHz) are not fully appropriate. The former because sensitivity limit of ~kT[11] and the latter because for complexes with high spins ($S > 1/2$) and high magnetic anisotropies (large *D* value) not all spin transitions will be observed. Also, torque magnetometry is not useful for non-crystalline samples. The most precise way to determine magnetic anisotropy in transition metal complexes is to perform continuous sweep in a broad range of magnetic field (using high magnetic fields) at different high frequencies (100 GHz–1 THz), applying so called high-field/high-frequency ESR (HF-ESR).

Here we present study of magnetic anisotropy in two new 1D coordination polymers, made of hetero-trinuclear repeating units: $\{SrCr_2(phen)_2(C_2O_4)_4\}\cdot H_2O$ (SrCrPhen) and $\{SrCr_2(bpy)_2(C_2O_4)_4(H_2O)\}\cdot 5H_2O$ (SrCrBpy), where phen = 1,10-phenantroline and bpy = 2,2'-bipyridine. In these complexes, two paramagnetic Cr(III) ions with spin $S = 3/2$ are bridged over oxalate groups and diamagnetic Sr(II) ions that break exchange interaction paths. Therefore, despite 1D crystal structures, these systems are magnetically 0D systems. Beside the structural and magnetic features, these complexes are additionally interesting because they could be used as single-source precursors for the formation of Sr-Cr oxides. Continuing

[a] Ruđer Bošković Institute, Bijenička 54, 10000 Zagreb, Croatia.
[b] University of Zagreb, Faculty of Science, Department of Physics, Bijenička 32, 10000 Zagreb, Croatia.
[c] IFW Dresden, Institute for Solid State Research, Helmholtzstrasse 20, D-01069 Dresden, Germany.
*E-mail: dzilic@irb.hr (D. Žilić)

Electronic Supplementary Information (ESI) available: [CIF files; Additional crystallographic information; TG/DTA curves; XPRD data of $\alpha$-$SrCr_2O_4$ obtained by heat treatment of SrCrBpy; CCDC 1579374-1579375]. See DOI: 10.1039/x0xx00000x

to our previous results when we studied calcium-analogues CaCrPhen and CaCrBpy complexes[12-14] here we present how, performing multifrequency HF-ESR spectroscopy, in combination with commonly used characterization techniques: X-ray diffraction, magnetic susceptibility and X-band ESR measurements, quantitatively good magneto-structural correlations could be established.

## Results and discussion

### Structural analysis

Compounds SrCrPhen and SrCrBpy are 1D coordination polymers consisting of similar repeating units, hetero-trinuclear species of the formula $\{Sr[Cr(phen)(C_2O_4)_2]_2\}$ (Fig. 1) and $\{Sr(H_2O)[Cr(bpy)(C_2O_4)_2]_2\}$ (Fig. 2), respectively. SrCrPhen has analogue chemical formula to previously published CaCrPhen (Sr instead of Ca), but two compounds are not isostructural ($P\bar{1}$ *vs.* $P2_1/n$).[13] SrCrBpy compound accommodates significantly larger number of water molecules compared to calcium analogue structure CaCrBpy ($P\bar{1}$), crystalizing as pentahydrate in $P2_1/c$ space group.[12-14] Moreover, geometry around the strontium ion in SrCrBpy is different to that in SrCrPhen, where along with the four oxalate groups additional water molecule is coordinated. In each compound there are two crystallographicaly independent chromium(III) ions with distorted octahedral geometry, comprising four O atoms from the two bis(bidentate) oxalate groups and two N atoms from a bidentate phen/bpy ligand (Fig. 1 and 2). The Cr–O and Cr–N distances, and angles describing the coordination octahedra are given in Tables 1 and 2, for SrCrPhen and SrCrBpy complexes, respectively.

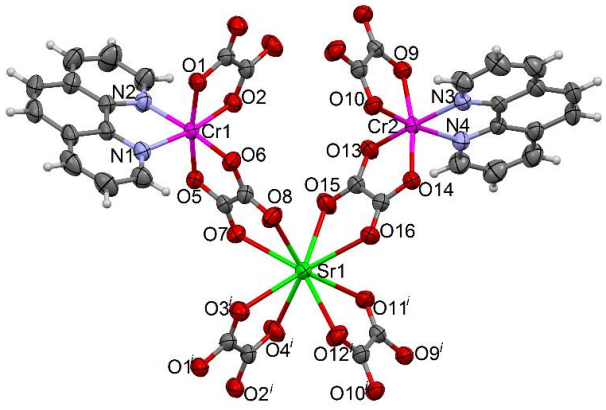


**Fig. 1** The drawing of the asymmetric unit in SrCrPhen with the atom numbering scheme of coordination sphere around metal centres. Crystallization water molecule is omitted. Displacement ellipsoids are drawn for the probability of 50% and hydrogen atoms are shown as spheres of arbitrary radii. Symmetry operator: (*i*) 1 + *x*, *y*, *z*.

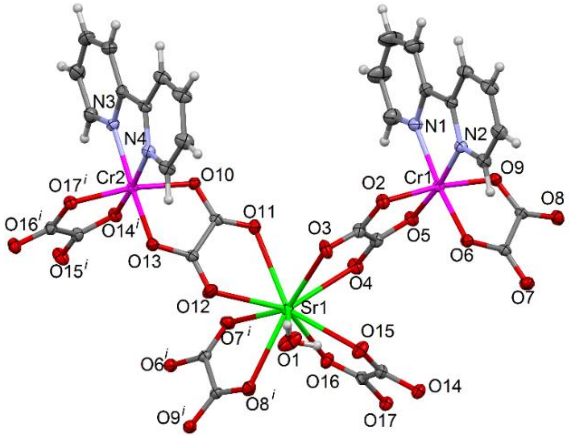


**Fig. 2** The drawing of the asymmetric unit in SrCrBpy with the atom numbering scheme of coordination sphere around metal centres. Crystallization water molecules are omitted. Displacement ellipsoids are drawn for the probability of 50% and hydrogen atoms are shown as spheres of arbitrary radii. Symmetry operator: (*i*) –*x*, 1/2 + *y*, 3/2 – *z*.

**Table 1** Molecular geometry and differences between corresponding lengths and angles in two octahedra of SrCrPhen complex.

| Cr1 octahedron | | Cr2 octahedron | | Difference |
|---|---|---|---|---|
| | | Angle Θ (°) | | |
| **N1-Cr1-O2** | 170.48 | N4-Cr2-O10 | 171.56 | \|ΔΘ\|=1.08 |
| O1-Cr1-O5 | 170.69 | O9-Cr2-O14 | 169.38 | \|ΔΘ\|=1.31 |
| N2-Cr1-O6 | 172.64 | N3-Cr2-O13 | 174.49 | \|ΔΘ\|=1.85 |
| | | | | Sum \|ΔΘ\|=4.24 |
| | | Bond distance x (Å) | | |
| Cr1-N1 | 2.069 | Cr2-N4 | 2.078 | \|Δx\|=0.009 |
| Cr1-N2 | 2.068 | Cr2-N3 | 2.077 | \|Δx\|=0.009 |
| Cr1-O1 | 1.957 | Cr2-O9 | 1.976 | \|Δx\|=0.019 |
| Cr1-O2 | 1.959 | Cr2-O10 | 1.956 | \|Δx\|=0.003 |
| Cr1-O5 | 1.965 | Cr2-O14 | 1.966 | \|Δx\|=0.001 |
| Cr1-O6 | 1.964 | Cr1-O13 | 1.959 | \|Δx\|=0.005 |
| | | | | Sum \|Δx\|=0.046 |

**Table 2** Molecular geometry and differences between corresponding lengths and angles in two octahedra of SrCrBpy complex.

| Cr1 octahedron | | Cr2 octahedron | | Difference |
|---|---|---|---|---|
| | | Angle Θ (°) | | |
| N1-Cr1-O6 | 173.09 | N3-Cr2-O13 | 173.78 | \|ΔΘ\|=0.69 |
| O2-Cr1-O9 | 172.05 | O10-Cr2-O17 | 169.54 | \|ΔΘ\|=2.51 |
| N2-Cr1-O5 | 172.95 | N4-Cr2-O14 | 172.94 | \|ΔΘ\|=0.01 |
| | | | | Sum \|ΔΘ\|=3.21 |
| | | Bond distance x (Å) | | |
| Cr1-N1 | 2.062 | Cr2-N3 | 2.052 | \|Δx\|=0.01 |
| Cr1-N2 | 2.049 | Cr2-N4 | 2.053 | \|Δx\|=0.004 |
| Cr1-O2 | 1.970 | Cr2-O17 | 1.977 | \|Δx\|=0.007 |
| Cr1-O5 | 1.968 | Cr2-O14 | 1.954 | \|Δx\|=0.014 |
| Cr1-O6 | 1.966 | Cr2-O13 | 1.961 | \|Δx\|=0.005 |
| Cr1-O9 | 1.966 | Cr1-O10 | 1.979 | \|Δx\|=0.013 |
| | | | | Sum \|Δx\|=0.053 |

The crystal structures of SrCrPhen and SrCrBpy are driven with aromatic stacking interactions accomplished between pyridyl groups sticking from neighbouring heterometallic chains (Fig. 3). Additionally, water molecules together with the oxalate moieties favour the hydrogen bonding formation, especially in SrCrBpy where one coordinated and five crystallization water molecules are present. Fig. S1 in Electronic Supplementary Information (ESI) shows how these water molecules fill the channels remaining between the π-stacked coordination polymers, interconnecting them further with hydrogen bonds into a 3D supramolecular assembly. Details on stacking interactions and hydrogen bonding geometry are given in Tables S1 and S2 in ESI, respectively.

**Thermal Analysis**

A simultaneous TG and DTA analysis of compounds SrCrPhen and SrCrBpy was carried out in a stream of nitrogen. The data obtained from the thermal analysis are supported by the chemical and single crystal X-ray diffraction analysis, confirming purity of the bulk samples. The TG and DTA curves of compounds SrCrPhen and SrCrBpy are presented in Fig. S2, along with the thermoanalytical data given as inset. Compound SrCrBpy starts to decompose almost immediately after the beginning of heating due to large number of crystallization water molecules. Even though water molecules start to evaporate with the beginning of heating, to fully remove them sample needs to be heated up to 200°C in SrCrPhen and 250°C in SrCrBpy. Aromatic ligands and oxalates are decomposed in the following steps, accompanied with two stronger exothermic peaks at DTA curve. Elimination of organic part in SrCrPhen requires even 100°C higher temperature than in SrCrBpy, which is probably related to presence of bulkier phen ligand, and absence of oxygen for conversion to gaseous nitrogen and carbon oxides. Mass rest at 1300°C in both samples almost perfectly matches to calculated value for $SrCr_2O_4$. However, as thermal analyser is not perfectly isolated system, we have observed that during the cooling part of the Cr(III) is being oxidised to Cr(VI). Powder X-ray diffraction analysis performed on thermal decomposition residue obtained by heat treatment of SrCrBpy at 1300°C, and then cooled to room temperature, along with the major product α-$SrCr_2O_4$ (78%) detected the presence of $SrCrO_4$ (10%) and $Cr_2O_3$ (12%). The result of Rietveld refinement is shown in Fig. S3. The structure of mixed Sr-Cr oxide, which exhibits quasi-two-dimensional and frustrated magnetic behaviour, is characterized by the layers of edge-shared $CrO_6$ octahedra, separated by Sr cations in trigonal prismatic coordination[15, 16] (inset Fig. S3). This suggests that both complexes, with additional tuning of thermal treatment parameters, might be useful single-source molecular precursor for the preparation of α-$SrCr_2O_4$.

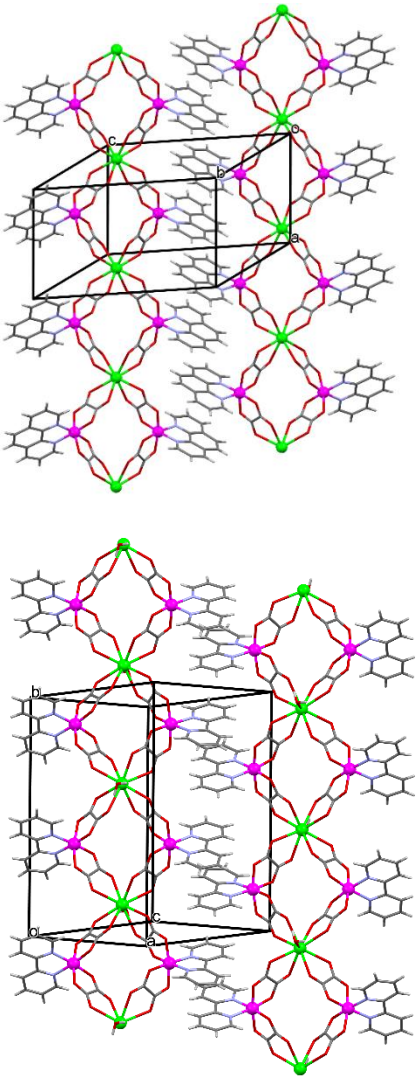


**Fig. 3** Stacking interactions between neighbouring 1D double chains in the crystal packing of SrCrPhen (up) and SrCrBpy (down).

### Magnetization

The magnetization $M(T)$ of SrCrPhen and SrCrBpy was measured as a function of temperature in different magnetic fields $H$. The representative magnetic susceptibility curves $\chi(T) = M(T)/H$ at $H$ = 1 kOe are shown in Fig. 4. Measurements in the ZFC (zero-field-cooled) and FC (field-cooled) modes yielded identical results within experimental uncertainty. The $\chi(T)$ are smooth and feature no peaks even in the smallest fields, down to 2 K. Also, the field dependences of the magnetization, $M(H)$, are reversible at all measured temperatures down to 2 K. Such a typical paramagnetic behaviour of $M(T)$ and $M(H)$ indicates the absence of long-range magnetic order or spin freezing in the studied compounds. The magnetic susceptibility $\chi$ was calculated for a field of 1 kOe (Fig. 4) in the framework of the Van Vleck type of analysis, which is fully applicable in this case given the observed linearity of $M(H)$ at different temperatures even for fields considerably larger than 1 kOe.

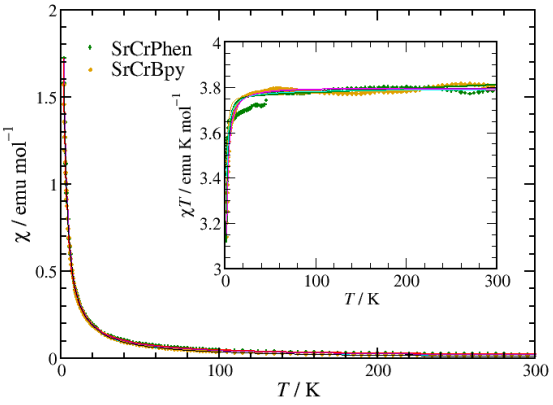


**Fig. 4** The temperature dependences of the molar magnetic susceptibility measured in the field of 1 kOe. Solid lines represent the fitting curves.

Due to the paramagnetic-like behaviour and in accordance with the known crystallographic structures of SrCrPhen and SrCrBpy complexes, magnetic susceptibility was modelled in the powder approximation assuming the non-interacting Cr(III) ions with spin $S$ = 3/2 and including the ZFS type of single ion anisotropy with neglected rhombic term. Therefore, the well-known formulas[2] were used:

$$\chi(T) = (\chi_z + 2\chi_x)/3 \qquad (1)$$

where

$$\chi_z = (Ng^2\beta^2)/(4kT) \cdot (1 + 9exp(-2D/kT))/(1 + exp(-2D/kT)) \qquad (2)$$

$$\chi_x = (Ng^2\beta^2)/(kT) \cdot (1 + 3kT/4D(1 - exp(-2D/kT)))/(1 + exp(-2D/kT)). \qquad (3)$$

Here, $g$ is the $g$-factor, $D$ is the axial ZFS parameter, with $N$ being Avogadro number, $k$ is the Boltzmann constant and $\beta$ is the Bohr magneton. The best fitting of calculated curves over the measured data was obtained for the parameters presented in Table 3.

**Table 3** $g$-values and axial ZFS parameters $D$ obtained from the magnetization analyses.

| Complex | SrCrPhen | | SrCrBpy | |
|---|---|---|---|---|
| Analysis | From $\chi(T)$ | From $\chi T(T)$ | From $\chi(T)$ | From $\chi T(T)$ |
| $g$ | 1.975(7) | 2.003(6) | 1.991(3) | 2.002(4) |
| $\lvert D \rvert$ (K) | 1.60(8) | 2.14(6) | 2.98(4) | 3.19(1) |

The root mean square (RMS) relative errors of the models are between 0.002 and 0.02 and the results of $\chi(T)$ and $\chi T(T)$ analysis are similar confirming the consistency of the applied model. In all calculations, we omitted the region of the data where irregular behaviour is observed for SrCrPhen. The obtained values of $g$-factors are in accordance with the usual value for Cr(III).[17-20] The values of the axial ZFS term $D$ are somewhat higher than those obtained from the ESR analysis, due to the neglected rhombic ZFS parameter $E$, and averaged contribution of two magnetically non-equivalent Cr(III) ions.

Finally, the values of the magnetization and a good agreement between the fitted curves and the measured data confirm the assumption of the isolated, non-interacting Cr(III) ions. Obviously, the diamagnetic Sr(II) ions break the exchange interaction paths between the Cr ions (the nearest Cr···Cr distance in the chains of SrCrPhen and SrCrBpy is 6.6 and 7.4 Å, respectively). Also, other interaction paths among neighbouring Cr(III) ions can be excluded based on the experimental results.

### ESR spectroscopy

ESR spectroscopy was performed on polycrystalline samples ground into powder. During the measurements in high-magnetic fields, small grains of the samples self-oriented in the field.

#### X-band ESR spectroscopy

The temperature dependence of the X-band (10 GHz) ESR spectra of the investigated complexes is shown in Fig. 5. The intensity of the ESR signals increases with decreasing temperature, in agreement with the paramagnetic behaviour of the static susceptibility (cf. Fig. 4). For SrCrBpy only one strong line is dominating in the spectrum while for the SrCrPhen complex, the corresponding line is split. The observed lines could be assigned to the central ESR allowed transition $m_s$ = -1/2 <-> $m_s$ = 1/2 of the Cr(III) ions with spin $S$ = 3/2. The other two Cr(III) allowed transitions: $m_s$ = -3/2 <-> $m_s$ = -1/2 and $m_s$ = 1/2 <-> $m_s$ = 3/2 could not be detected at the X-band but they are observed at higher frequencies using the HF-ESR setup (see below).[14, 17, 18, 20]

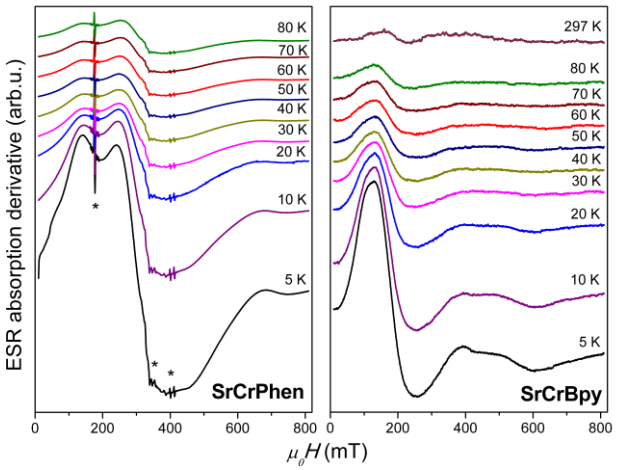


**Fig. 5** Temperature dependence of X-band ESR spectra of SrCrPhen and SrCrBpy complexes. The narrow lines marked with asterisks originate from ESR cavity.

### HF-ESR spectroscopy

The HF-ESR spectra of SrCrPhen and SrCrBpy complexes at several selected high frequencies in the range 83-415 GHz, together with the frequency $\nu$ vs. resonant magnetic field $H_{res}$ diagram, are shown in Fig. 6 and 7, respectively. The spectra of SrCrBpy consist of three doublet lines, as can be seen in Fig. 7, similar to the spectra of CaCrBpy.[14] However, unlike the spectra of CaCrPhen complex[14] that exhibits three ESR lines at all measured frequencies, SrCrPhen shows more complicated behaviour, as can be seen in Fig. 6. Besides the weak lines associated with the forbidden transitions $\Delta m_s > 1$, only three main lines are observed at the lowest frequency of 83 GHz. In contrast, at higher frequencies of 166, 249, 332 and 415 GHz these main lines are split and altogether five lines are observed. Such a behaviour is visible also in the temperature dependences of spectra, recorded at two selected frequencies, shown in Fig. 8 and 9. The three doublets (six lines) can be seen for the SrCrBpy complex at both excitation frequencies and at all measured temperatures (Fig. 9). However, for SrCrPhen the splitting of the three main lines is observed only at a higher frequency (249 GHz) and at a lower temperature (Fig. 8). Therefore, for the SrCrPhen and SrCrBpy complexes, five and six resonance branches $\nu(H)$ do exist, respectively, marked with different colours in Fig. 6 and 7. From these resonance branches, the first estimation of $g$-values as well as magnetic anisotropy gap $\Delta$ for Cr(III) ions could be obtained [14] according to the relation $h\nu = \Delta + g\,\beta\,H$, and these values are indicated in the Fig. 6 and 7. The $g$-values for the forbidden transition ($g \approx 3.8$) is approximately twice as for allowed transition ($g \approx 2$), as it is expected for the case of $\Delta m_s = \pm 2$ .

Additionally, as it can be seen in Fig. 8 and 9, with lowering the temperature the lower-field ESR lines progressively gain in intensity in expense of the lines at higher fields. This points at the easy-axis type of magnetic anisotropy in the complexes, i.e. that the doublet $|m_s> = |\pm 3/2>$ of the $S = 3/2$ spin multiplet of Cr(III) is the ground state and the doublet $|m_s> = |\pm 1/2>$ lies at a higher energy. For a given constant temperature this effect of the redistribution of the spectral weight is more prominent at higher frequencies and correspondingly stronger magnetic fields (cf. left and right panels in Fig. 8 and 9). Indeed, the Zeeman splitting of the doublet $|m_s> = |\pm 3/2>$ is twice larger as of the doublet $|m_s> = |\pm 1/2>$, rendering the ground state level $|m_s> = |-3/2>$ much higher populated at low temperatures and strong fields as compared to other states at higher energies. Therefore, the low-field line corresponding to the transition $m_s = -3/2 <-> m_s = -1/2$ is most intense in this regime. Note that the two weak lines in the spectra of SrCrPhen at the lowest measured frequency of 83 GHz (Fig. 8, left) at magnetic fields ≈ 0.73 and 0.92 T, are the previously mentioned forbidden transitions.

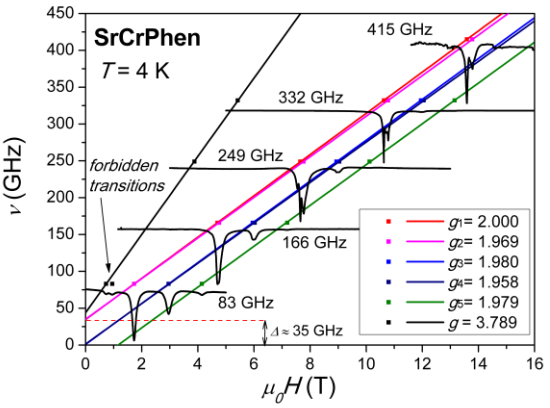


**Fig. 6** Frequency dependence of the oriented powder SrCrPhen spectrum at 4 K.

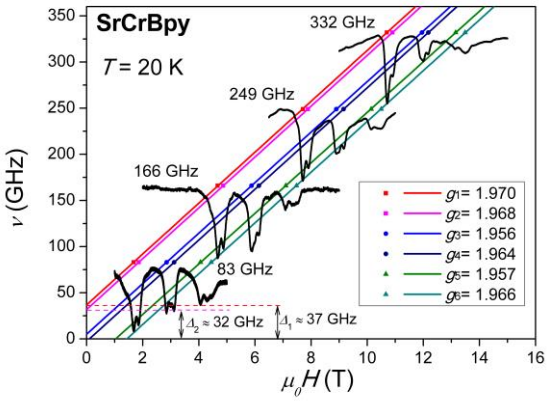


**Fig. 7** Frequency dependence of the oriented powder SrCrBpy spectrum at 20 K.

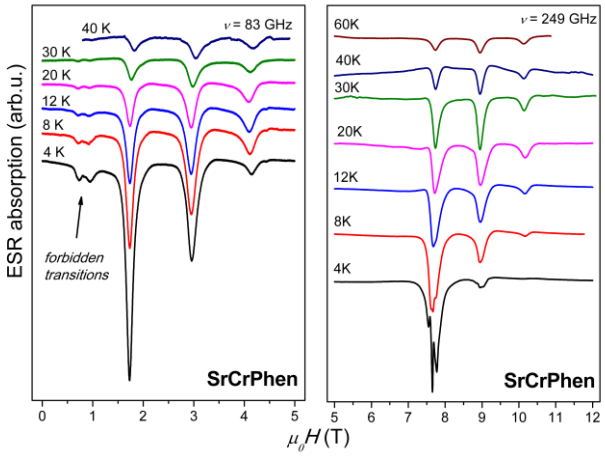


**Fig. 8** Temperature dependence of ESR spectra of SrCrPhen complexes at indicated frequencies.

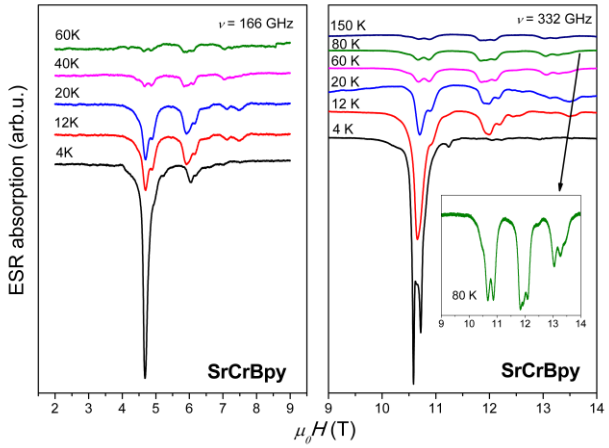


**Fig. 9** Temperature dependence of ESR spectra of SrCrBpy complexes at indicated frequencies.

## Simulation

To describe the obtained spectra, the following form of the spin-Hamiltonian for paramagnetic Cr(III) ions with spin $S$=3/2 was used:[2, 7, 14, 20]

$$\boldsymbol{H} = g\beta \boldsymbol{B}\cdot\boldsymbol{S} + \boldsymbol{D}[\boldsymbol{S}_z^2 - \boldsymbol{S}(\boldsymbol{S}+\boldsymbol{1})/\boldsymbol{3}] + \boldsymbol{E}(\boldsymbol{S}_x^2 - \boldsymbol{S}_y^2). \quad (4)$$

Here all parameters have their usual meaning.
The $g$-factor is approximated with the isotropic value, according to the literature data for Cr(III) ions in a distorted octahedral coordination.[17-21] The axial ZFS parameter $D$ is connected with the parameter $\Delta$ obtained from the $y$-intercept of the most left resonance branch ν vs. $H$, as indicated in Fig. 6 and 7 as:[10, 14, 22]

$$|\boldsymbol{D}| = \boldsymbol{\Delta}/[\boldsymbol{S}^2 - (\boldsymbol{S}-\boldsymbol{1})^2] = \boldsymbol{\Delta}/\boldsymbol{2}\,. \quad (5)$$

The sign of the parameter $D$ is negative (i.e. the doublet $|m_s\rangle = |\pm 3/2\rangle$ is the ground state) as it follows from the above discussion of the temperature-driven changes of the relative intensities of the spectral lines (Fig. 8 and 9). This is also consistent with the observed self-orientation of powder grains in high-magnetic fields. To obtain more accurate values of the spin-Hamiltonian parameters (SH parameters), the spectral simulations were performed, using the EasySpin software.[23] For the X-band spectra powder simulations were carried out, while for the HF-ESR spectra single crystal simulations were performed for the case when the external magnetic field $H$ is parallel with the magnetic easy axis $z$. The simulated spectra are presented in Fig. 10 and 11 revealing a good agreement with the experiment. The obtained SH parameters are given in Table 4.

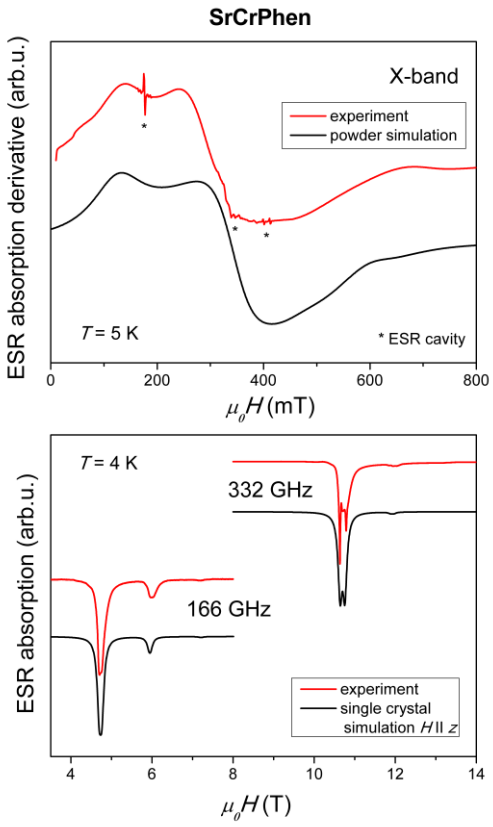


**Fig. 10** Experimental and simulated spectra of SrCrPhen complex at three different frequencies: 9.6 and 166 and 332 GHz.

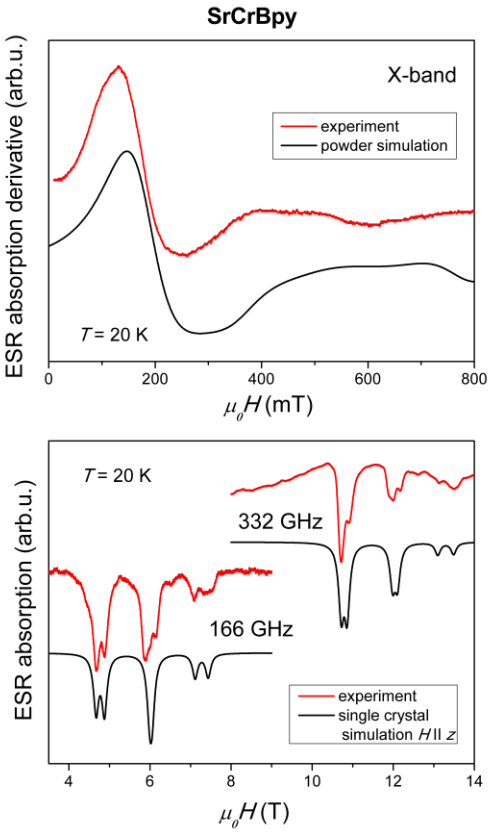


**Fig. 11** Experimental and simulated spectra of SrCrBpy complex at three different frequencies: 9.6 and 166 and 332 GHz.

**Table 4** The spin-Hamiltonian parameters obtained from the simulations.

| Complex | SrCrPhen | | SrCrBpy | |
|---|---|---|---|---|
| *g* | 1.980 | 1.995 | 1.960 | 1.980 |
| *D* (K) | -0.82 | -0.84 | -0.91 | -0.74 |
| \|*E*\| (K) | 0.26 | 0.26 | 0 | 0 |

### Magneto-structural correlations

In Table 4 one can compare the two sets of the SH parameters *g*, *D* and |*E*|, that were obtained from the simulation of the SrCrPhen and SrCrBpy ESR spectra. The rhombic parameter |*E*| is zero for the SrCrBpy complex while for the SrCrPhen complex it has a value of 0.26 K. The sign of *E* has no physical meaning[24] but the role of the parameter *E* could be at best seen in the X-band spectra where non-zero *E* produces a splitting of the central line of the SrCrPhen spectra.

The obtained two sets of the SH parameters reflect the existence of two crystallographically independent chromium ions Cr1 and Cr2 in the asymmetric unit of the complexes, as it is explained in the structural analysis. The chromium ions have distorted octahedral geometries due to irregular positions of the neighbouring two nitrogen and four oxygen ions, as can be seen in Fig. 1 and 2. Two crystalographically and also magnetically inequivalent chromium octahedra are shown in Fig. 12. In this figure, the local, approximately two-fold rotation axes (black rods) that pass through the Cr ions and through the middle of the edges of octahedra, are highlighted and they present the easy axes of magnetization (magnetic *z*-axes). One can see that these axes for the two octahedra are approximately collinear which explains why strong magnetic field can orient crystalline particles of the investigated complexes.[14, 17]

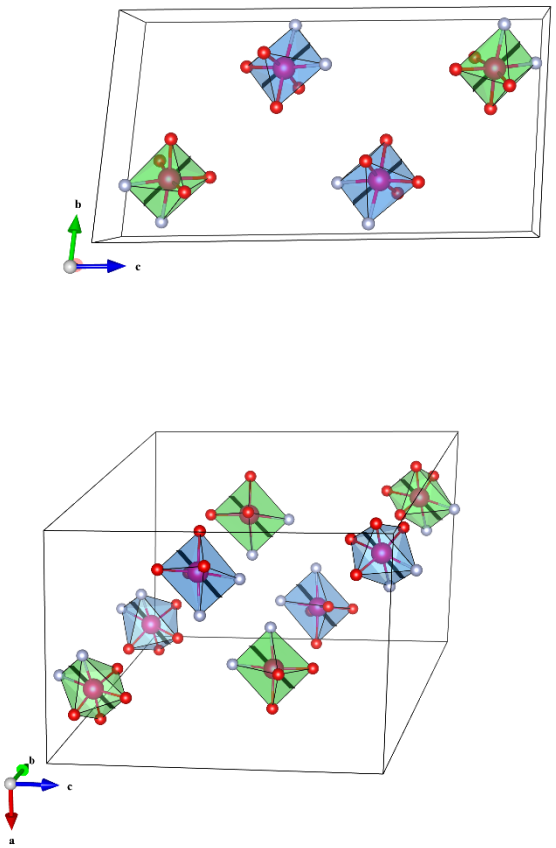


**Fig. 12** Arrangement of Cr1 (coloured in blue) and Cr2 (coloured in green) coordination polyhedra in the unit cell of SrCrPhen (up) and SrCrBpy (down). The local, approximate two-fold rotation axis (black rod) passes through the Cr atom and through the middle of the edges of octahedron, which connect two nitrogen (blue) atoms and two oxygen (red) atoms opposite to nitrogen atoms.

Bond distances, *x*, and angles, *Θ*, in two chromium octahedra are given in Tables 1 and 2. If we compare the sums of the differences of the bond distances, |Δx|, and of the angles, |ΔΘ| in two octahedra, for the SrCrPhen and SrCrBpy complexes with the corresponding values obtained for the calcium analogues

CaCrPhen and CaCrBpy[14] one observes an excellent correlation with the HF-ESR results. Namely, when the difference between two chromium octahedra is small (CaCrPhen) only three HF-ESR lines are detected and one set of SH parameters is sufficient to simulate the spectra. In contrast, when the difference between the chromium octahedra is bigger (CaCrBpy, SrCrPhen and SrCrBpy) the three HF-ESR lines are split and two sets of SH parameters are necessary for the successful simulations. For SrCrPhen the splitting was resolved at frequencies above 83 GHz. Additionally, the anisotropy in a hard magnetic plane (the plane perpendicular to the easy axis) described with the ZFS parameter *E*, is also reflected in structural parameters given in Tables 1 and 2.[14]

## Conclusions

Two 1D Sr(II)Cr(III) coordination polymers SrCrPhen and SrCrBpy were synthesized and characterized in detail by X-ray, thermal, magnetic susceptibility, X-band and HF-ESR studies. Single crystal X-ray analysis reveals double oxalate-bridged zigzag Sr-Cr chains. In each compound, there are two crystallographicaly independent Cr(III) ions with distorted octahedral geometry. Magnetic susceptibility shows paramagnetic behaviour of these complexes in agreement with the fact that diamagnetic Sr(II) ions break exchange interaction paths between the Cr(III) ions. X-band (10 GHz) ESR spectroscopy detects the central transition between energy levels of chromium ions with spin $S$ = 3/2. Performing multifrequency HF-ESR (83-415 GHz), all three allowed ESR transitions were detected and assigned.

Besides these findings, the main observation of this work is the detection of the splitting of the ESR lines at high frequencies. Using spectral simulations, we have concluded that the two sets of the spin-Hamiltonian parameters are necessary to describe these systems, due to existence of two magnetically non-equivalent Cr(III) ions in asymmetric units. The simulations show that Cr ions in SrCrPhen and SrCrBpy could be described by biaxial and uniaxial type of magnetic anisotropy, respectively, with small negative axial ZFS *D*-parameters ($D \approx -1$ K). This work, together with our previous investigation[14], show the advantages of HF-ESR for the establishment of the rational magneto-structural correlations in transition-metal complexes on the quantitative level.

## Experimental

**Materials and Physical Measurements.** The chemicals were purchased from commercial sources, and used without further purification. Elemental analyses for C, H and N were carried out using a Perkin Elmer Model 2400 microanalytical analyser. Thermal measurements were carried out on a Shimadzu DTG-60H analyser, in the range from room temperature (RT) to 1500°C, in the stream of the nitrogen, at a heating rate of 10°C $min^{-1}$.

**Synthesis of Compounds $\{SrCr_2(phen)_2(C_2O_4)_4\}\cdot H_2O$ (SrCrPhen) and $\{SrCr_2(bpy)_2(C_2O_4)_4(H_2O)\}\cdot 5H_2O$ (SrCrBpy).** An aqueous solution (8 mL) containing $Cr(NO_3)_3\cdot 9H_2O$ (0.4002 g; 1 mmol) and ligand (bpy = 0.1561 g or phen·$H_2O$ = 0.1982 g; 1 mmol) was refluxed for 40 minutes. To the hot reaction mixture an aqueous solution (5 mL) of $K_2(C_2O_4)\cdot H_2O$ (0.3685 g; 2 mmol) was added and the reflux was continued for further 30 minutes. A small amount of a violet precipitate that appeared during the refluxing was removed by filtration. To the clear solution, an aqueous solution (4 mL) of $Sr(NO_3)_2\cdot 4H_2O$ (0.2836 g; 1 mmol) was added dropwise. A red crystalline precipitate that formed immediately, was removed by filtration. From the clear solution, red plate-like crystals (SrCrPhen or SrCrBpy) started to form very soon. The process of crystallization was completed within one week, when the crystals were separated by filtration and dried in air. Yield: ~60% (for both compounds). Anal. Calcd for $C_{32}H_{18}SrCr_2N_4O_{17}$ (SrCrPhen): C, 41.68; H, 1.97; N, 6.07 (%). Found: C, 42.03; H, 2.08; N, 6.03 (%). Anal. Calcd for $C_{28}H_{28}SrCr_2N_4O_{22}$ (SrCrBpy): C, 34.88; H, 2.93; N, 5.81 (%). Found: C, 34.77; H, 2.90; N, 5.75 (%).

**Single Crystal X-ray Study.** Single crystal X-ray diffraction measurements were performed on an Oxford Diffraction Xcalibur Nova R (microfocus Cu tube) at room temperature for SrCrPhen and at 105.5(7) K for SrCrBpy. The program package CrysAlis PRO[25] was used for data reduction. Solution, refinement and analysis of the structures were performed using the programs integrated in the WinGX system.[26] The structure was solved using SIR92[27] and refined by the full-matrix least-squares method based on $F2$ against all reflections with SHELXL(2017-1).[28] Hydrogen atoms bound to C atoms were modelled as riding entities using the AFIX command, while those bound to O were located in a difference Fourier map and refined with the following restraints: geometry of water molecules was constrained to $d$(O–H) = 0.90(2) Å and $d$(H···H) = 1.50(4) Å. Molecular geometry calculations were performed by PLATON,[29] and molecular graphics were prepared using ORTEP-3,[26] CCDC-Mercury[30] and VESTA[31]. The crystal data, experimental conditions and final refinement parameters for the structure reported are summarized in Table 5 Crystallographic data for this paper can be obtained free of charge *via* www.ccdc.cam.ac.uk/conts/retrieving.html (or from the Cambridge Crystallographic Data Centre, 12, Union Road, Cambridge CB2 1EZ, UK; fax: +44 1223 336033; or deposit@ccdc.cam.ac.uk). CCDC 1579374-1579375 contains the supplementary crystallographic data for this paper.

**Magnetization measurement.** Magnetization $M$ of the powder samples was measured with a MPMS-5 commercial magnetometer equipped with superconducting quantum interferometer device (SQUID). The measurements of the samples were corrected by taking into account the ampoule with capton-tape and temperature-independent contributions. Additionally, the field dependences of magnetization, $M(H)$, including magnetic hysteresis loops, were measured at several stable temperatures in fields up to 50 kOe. The temperature dependence of magnetic susceptibility in the interval 2-300 K was calculated for 1000 Oe magnetic field.

**ESR spectroscopy.** X-band ESR experiments were performed with Bruker spectrometers: Elexsys 580 FT/CW and EMX for SrCrPhen and SrCrBpy compounds, respectively. The spectra

 

were recorded from room down to liquid helium temperature with a magnetic field modulation amplitude of 0.3 mT and frequency of 100 kHz. HF-ESR experiments were carried out with a homemade spectrometer based on Millimeterwave Vector Network Analyzer (AB Millimetre, Paris) that produces millimetre- and submillimetre microwaves and allows phase locked detection of a signal. The HF-ESR spectrometer uses magnetocryostat (Oxford Instruments Ltd.) with magnetic fields 0-16 T. For more details, see Ref. [32] The spectra were recorded in the temperature range 4-150 K, at several selected frequencies of 83, 166, 249, 332 and 415 GHz.

**Table 5.** Crystallographic data and structure refinement details for SrCrPhen and SrCrBpy.

| Compound | **SrCrPhen** | **SrCrBpy** |
|---|---|---|
| empirical formula | $C_{32}H_{18}SrCr_2N_4O_{17}$ | $C_{28}H_{28}SrCr_2N_4O_{22}$ |
| formula wt./g mol$^{-1}$ | 922.12 | 964.16 |
| space group | $P\bar{1}$ | $P2_1/c$ |
| *a*/Å | 9.2532(3) | 11.756(5) |
| *b*/Å | 10.7380(4) | 18.408(5) |
| *c*/Å | 18.8419(6) | 16.529(5) |
| *α*/° | 84.973(3) | 90 |
| *β*/° | 87.148(3) | 95.107(5) |
| *γ*/° | 69.039(3) | 90 |
| Z | 2 | 4 |
| *V*/Å$^3$ | 1741.19(11) | 3563.0(2) |
| $D_{calc}$/g cm$^{-3}$ | 1.759 | 1.798 |
| $\mu$/mm$^{-1}$ | 7.793 | 7.749 |
| *Θ* range/deg | 4.42–76.19 | 3.6–75.81 |
| *T*/K | 293(2) | 105.5(7) |
| reflections collected | 21768 | 19801 |
| independent reflections | 7118 | 7362 |
| observed reflections ($I \geq 2\sigma$) | 5977 | 6918 |
| $R_{int}$ | 0.0528 | 0.0364 |
| *R (F)* | 0.0505 | 0.0378 |
| $R_w$ ($F^2$) | 0.1373 | 0.1031 |
| goodness of fit | 1.044 | 1.030 |
| no. of parameters, estraints | 508, 0 | 557, 16 |
| $\Delta\rho_{max}$, $\Delta\rho_{min}$/e Å$^{-3}$ | 1.468; –1.082 | 0.719; –1.137 |

## Conflicts of interest

There are no conflicts to declare.

## Acknowledgements

This research was supported in part by Croatian Science Foundation (1108, IP-2014-09-4079 and UIP-2014-09-8276). Authors are grateful to dr. K. Molčanov and dr. Z. Štefanić from RBI for single-crystal data collection. The postdoc stay of D. Žilić at the IFW-Dresden was supported by Croatian Science Foundation (Project 02.03/164).

## Notes and references

1. D. W. Stephan, *Coordination Chemistry Reviews*, 1989, **95**, 41-107.
2. O. Kahn, *Molecular Magnetism*, Wiley, 1993.
3. V. G. Makhankova, A. O. Beznischenko, V. N. Kokozay, R. I. Zubatyuk, O. V. Shishkin, J. Jezierska and A. Ozarowski, *Inorganic Chemistry*, 2008, **47**, 4554-4563.
4. R. J. Kuppler, D. J. Timmons, Q.-R. Fang, J.-R. Li, T. A. Makal, M. D. Young, D. Yuan, D. Zhao, W. Zhuang and H.-C. Zhou, *Coordination Chemistry Reviews*, 2009, **253**, 3042-3066.
5. D. Gatteschi, R. Sessoli and J. Villain, *Molecular Nanomagnets*, Oxford University Press, 2006.
6. J.-N. Rebilly, L. Catala, G. Charron, G. Rogez, E. Riviere, R. Guillot, P. Thuery, A.-L. Barra and T. Mallah, *Dalton Transactions*, 2006, 2818-2828.
7. A. Abragam and B. Bleaney, *Electron Paramagnetic Resonance of Transition Ions*, Clarendon Press, Oxford, 1970.
8. M. Mostafanejad, *International Journal of Quantum Chemistry*, 2014, **114**, 1495-1512.
9. Y.-F. Deng, T. Han, Z. Wang, Z. Ouyang, B. Yin, Z. Zheng, J. Krzystek and Y.-Z. Zheng, *Chemical Communications*, 2015, **51**, 17688-17691.
10. A. Das, K. Gieb, Y. Krupskaya, S. Demeshko, S. Dechert, R. Klingeler, V. Kataev, B. Büchner, P. Müller and F. Meyer, *Journal of the American Chemical Society*, 2011, **133**, 3433-3443.
11. A. Bencini and D. Gatteschi, *Electron Paramagnetic Resonance of Exchange Coupled Systems*, Springer, Berlin, Heidelberg, 1990.
12. L. Androš, M. Jurić, K. Molčanov and P. Planinić, *Dalton Transactions*, 2012, **41**, 14611-14624.
13. L. Androš, M. Jurić, J. Popović, D. Pajić, K. Zadro, K. Molčanov, D. Žilić and P. Planinić, *European Journal of Inorganic Chemistry*, 2014, **2014**, 5703-5713.
14. D. Žilić, L. Androš, Y. Krupskaya, V. Kataev and B. Büchner, *Applied Magnetic Resonance*, 2015, **46**, 309-321.
15. S. E. Dutton, E. Climent-Pascual, P. W. Stephens, J. P. Hodges, A. Huq, C. L. Broholm and R. J. Cava, *Journal of Physics: Condensed Matter*, 2011, **23**, 246005.
16. L. Zhao, T.-W. Lan, K.-J. Wang, C.-H. Chien, T.-L. Hung, J.-Y. Luo, W.-H. Chao, C.-C. Chang, Y.-Y. Chen, M.-K.

Wu and C. Martin, *Physical Review B*, 2012, **86**, 064408.
17. N. Novosel, D. Žilić, D. Pajić, M. Jurić, B. Perić, K. Zadro, B. Rakvin and P. Planinić, *Solid State Sciences*, 2008, **10**, 1387-1394.
18. M. Jurić, P. Planinić, D. Žilić, B. Rakvin, B. Prugovečki and D. Matković-Čalogović, *Journal of Molecular Structure*, 2009, **924–926**, 73-80.
19. M. Jurić, L. Androš Dubraja, D. Pajić, F. Torić, A. Zorko, A. Ozarowski, V. Despoja, W. Lafargue-Dit-Hauret and X. Rocquefelte, *Inorganic Chemistry*, 2017, **56**, 6879-6889.
20. A. Carrington and A. D. McLachlan, *Introduction to magnetic resonance : with applications to chemistry and chemical physics*, Harper&Row, New York, 1967.
21. P. Chaudhuri, V. Kataev, B. Büchner, H.-H. Klauss, B. Kersting and F. Meyer, *Coordination Chemistry Reviews*, 2009, **253**, 2261-2285.
22. Y. Krupskaya, A. Alfonsov, A. Parameswaran, V. Kataev, R. Klingeler, G. Steinfeld, N. Beyer, M. Gressenbuch, B. Kersting and B. Büchner, *ChemPhysChem*, 2010, **11**, 1961-1970.
23. S. Stoll and A. Schweiger, *Journal of Magnetic Resonance*, 2006, **178**, 42-55.
24. J. A. Weil, J. R. Bolton and J. E. Wertz, *Electron paramagnetic resonance: Elementary theory and applications*, Wiley-interscience, New York, 1994.
25. Agilent, *Journal*, 2014.
26. L. Farrugia, *Journal of Applied Crystallography*, 2012, **45**, 849-854.
27. A. Altomare, G. Cascarano, C. Giacovazzo, A. Guagliardi, M. C. Burla, G. Polidori and M. Camalli, *Journal of Applied Crystallography*, 1994, **27**, 435.
28. G. Sheldrick, *Acta Crystallographica Section C*, 2015, **71**, 3-8.
29. A. Spek, *Acta Crystallographica Section D*, 2009, **65**, 148-155.
30. C. F. Macrae, P. R. Edgington, P. McCabe, E. Pidcock, G. P. Shields, R. Taylor, M. Towler and J. van de Streek, *Journal of Applied Crystallography*, 2006, **39**, 453-457.
31. K. Momma and F. Izumi, *Journal of Applied Crystallography*, 2011, **44**, 1272-1276.
32. C. Golze, A. Alfonsov, R. Klingeler, B. Büchner, V. Kataev, C. Mennerich, H. H. Klauss, M. Goiran, J. M. Broto, H. Rakoto, S. Demeshko, G. Leibeling and F. Meyer, *Physical Review B*, 2006, **73**, 224403.

 